FISEVIER

Contents lists available at ScienceDirect

Journal of Fluids and Structures

journal homepage: www.elsevier.com/locate/jfs



Porous panels with fixed ends lose stability by divergence



- Rozhin Hajian ^{a,b,*,1,2}, Justin W. Jaworski ^{c,3}
- ^a Harvard University, Cambridge, MA 02138, United States of America
- ^b Northeastern University, 360 Huntington Ave, Boston, MA 02115, United States of America
- ^c Lehigh University, Bethlehem, PA 18015, United States of America

ARTICLE INFO

Article history:
Received 31 May 2019
Received in revised form 20 November 2019
Accepted 29 November 2019
Available online xxxx

Keywords: Aeroelastic stability Panel flutter Singular integral equation

ABSTRACT

The aeroelastic stability of one-dimensional porous panels with a Darcy boundary condition on its surface is examined theoretically. Analytical and numerical analyses demonstrate that a porous panel in a uniform, single-sided, incompressible flow becomes aeroelastically unstable via divergence. This primary route of instability is identical to the well-known mechanism for non-porous panels. However, the divergence speed of a porous panel is always greater than the non-porous limit and increases with a dimensionless porosity parameter formed by the aeroelastic system. Various chordwise porosity distributions along the panel are also investigated, where the uniformly-porous panel is shown to be the most stable configuration. The generality and robustness of the primary divergence instability for porous panels is established analytically using a simple but general flutter analysis approach based on the Routh–Hurwitz stability criterion.

© 2019 Elsevier Ltd. All rights reserved.

1. Introduction

Vibrating panels are common sound sources in many engineering devices, such as passively-tuned vibration absorbers (TVA) (Jolly and Sun, 1994; Wright and Kidner, 2004), and continue to be the subject of active research (Jacobsen and Juhl, 2013; Fahy and Gardonio, 2007). The introduction of a mean flow adjacent to a flexible panel introduces the possibility of self-excited vibrations resulting from aeroelastic flutter. For one-dimensional panels fixed at each edge, the flutter boundary may be calculated using a set of appropriate structural equations coupled to non-circulatory aerodynamic theory. The non-circulatory forces in a steady flow have been previously studied for vibrating, flexible panels with different boundary conditions at the leading and trailing edges for both supersonic and subsonic flows (Ishii, 1965; Gislason, 1971; Weaver and Unny, 1970; Dugundji et al., 1963; Kornecki et al., 1976; Dowell, 1974; Hedgepeth, 1957; Datta and Gottenberg, 1975; Biot, 1956). Accordingly, the type of aeroelastic instability depends on the boundary conditions. In subsonic flow, panels fixed at both ends lose stability primarily by divergence, which has been studied both theoretically (Ishii, 1965; Gislason, 1971; Weaver and Unny, 1970; Dugundji et al., 1963; Kornecki et al., 1976) and experimentally (Gislason, 1971; Dugundji et al., 1963). For example, Dugundji et al. (1963) showed that divergence occurs for a simply-supported panel at a lower flow speed than for flutter. However, Weaver and Unny (1970) demonstrated that the critical flow speeds for divergence and flutter might be close together numerically, where one could imagine

^{*} Corresponding author at: Harvard University, Cambridge, MA 02138, United States of America. E-mail address: hajian@seas.harvard.edu (R. Hajian).

Postdoctoral Associate, School of Engineering and Applied Sciences.

² Lecturer, Mechanical and Industrial Engineering Department.

Assistant Professor, Department of Mechanical Engineering and Mechanics.

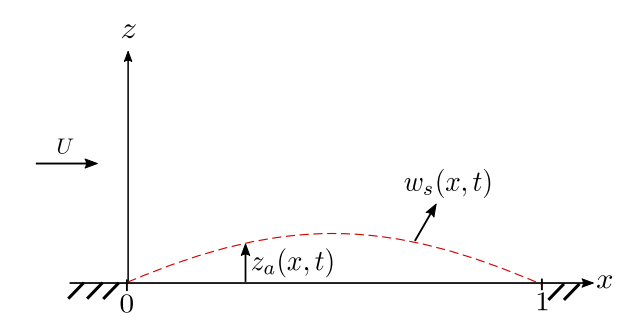


Fig. 1. Schematic of a thin, porous panel in one-sided flow of speed U that is undergoing unsteady deformations $z_a(x, t)$ and has seepage velocity $w_s(x, t)$. The coordinates are scaled by the panel chord length.

in a physical experiment that the primary divergence instability is accidentally bypassed and flutter oscillations of the secondary instability are observed instead. Flutter can be the true primary instability type in the case of other boundary conditions, such as cantilevered ends (Kornecki et al., 1976; Datta and Gottenberg, 1975), which has been confirmed experimentally (Kornecki et al., 1976). Similar results have also been obtained for an elastic strip pinned at one end and free at the other (Datta and Gottenberg, 1975).

The present work contributes to the panel flutter literature by incorporating the effects of panel porosity into aeroelastic stability predictions. The remainder of the paper is outlined as follows. Section 2 presents the structural and aerodynamic model equations. Section 3 suppresses the unsteady terms in the model equations to predict the divergence speed for panels with clamped and simply-supported end conditions. Section 4 carries out a generalized flutter analysis for panels with fixed ends to show that the introduction of porosity to a flexible panel does not change the primary route of instability: divergence. This section also develops a simple but general flutter analysis method to establish theoretically that the divergence primary instability mechanism is robust to variations in porosity. Conclusion for this work are summarized in Section 5.

2. Mathematical model

This section presents the structural and aerodynamic model equations used to study the aeroelastic instability of a thin panel with a two-dimensional, steady, incompressible flow on one side, as illustrated in Fig. 1. The linear equation of panel deformation is first presented and nondimensionalized. The non-circulatory aerodynamic forces on the panel are then described, which depend upon and are dynamically coupled to the elastic panel equation to furnish aeroelastic stability predictions.

2.1. Equation of panel motion

According to the Euler-Lagrange equation (Fox, 1950), the linear deformations $\bar{z}_a(x, t)$ of a one-dimensional, fluid-loaded panel of length l satisfy

$$D\frac{\partial^4 \bar{z}_a}{\partial \bar{x}^4} + \rho_s h \frac{\partial^2 \bar{z}_a}{\partial \bar{t}^2} + (p_u - p_l) = 0, \tag{1}$$

where D, ρ_s , and h denote the flexural rigidity, density, and panel thickness, respectively. The terms p_u and p_l represent the local pressures above and below the panel, respectively. All terms in Eq. (1) are dimensional quantities. By introducing the non-dimensional variables $x = \bar{x}/l$, $z_a = \bar{z}_a/l$, and $t = \bar{t}/\sqrt{\rho_s h l^4/D}$, Eq. (1) may be written as

$$\frac{\partial^4 z_a}{\partial x^4} + \frac{\partial^2 z_a}{\partial t^2} = \frac{\lambda^2}{2} p(x, t),\tag{2}$$

where $\lambda^2 = \rho U^2 l^3/D$ is a dimensionless dynamic pressure, and p(x, t) denotes the dimensionless pressure jump (lower minus upper, normalized by $\frac{1}{2}\rho U^2$) across the panel.

2.2. Non-circulatory pressure distribution

The classical work of Bisplinghoff et al. (1996) and Theodorsen (1949) separates the unsteady fluid forces due to harmonic motions of a thin deforming body (e.g., an airfoil or elastic panel) into circulatory and non-circulatory parts, which are related to the unsteady shedding of vorticity into the wake and the hydrodynamic sloshing of fluid about the body, respectively. Leonard and Roshko (2001) argue that this description of unsteady fluid forces holds also for real fluid flows, where inviscid theory continues to describe the non-circulatory contributions that depend solely on the geometry and kinematics of the solid body. Corkery et al. (2019) confirm this point experimentally for viscous and separated

flows and demonstrate that all unsteady force effects due to viscosity can be ascribed to circulatory flow effects. These circulatory effects may be modeled by a bound vorticity sheet on the body together with the free vorticity in the field and wake (Graham et al., 2017). Vorticity shed into the wake by the panel must be accounted for in the case of a free trailing edge (Kornecki et al., 1976) by imposition of the Kutta condition, which itself arises from viscous flow considerations near an edge. However, a vibrating panel with ends embedded in a solid surface does not produce a vortical wake in the present context of inviscid flow modeling. Therefore, only non-circulatory fluid forces act on the baffled panel in the model problem illustrated in Fig. 1. The non-circulatory pressure distribution on a panel may be modeled equivalently as either a distribution of sources (Bisplinghoff et al., 1996) (as in the present work) or as a distinct sheet of bound vorticity on the panel whose net circulation is zero at all times (Leonard and Roshko, 2001; Eldredge, 2010; Graham et al., 2017).

The present study connects the theoretical fluid analysis in Hajian and Jaworski (2019) to the structural dynamics of vibrating porous panels. Consider a panel with porosity distribution R(x) and the dimensionless porosity parameter, which depends on the flow and porosity of the airfoil material, $\delta = \rho UC$ (Hajian and Jaworski, 2015, 2017b), where C is the porosity coefficient. The product of the porosity coefficient, C, and porosity distribution, R(x), can be defined based on the physical properties of the airfoil and surrounding fluid as

$$CR(x) = \frac{\kappa}{ud}. (3)$$

The symbol μ denotes the fluid viscosity, and κ and d represent the permeability and thickness of the porous material, respectively, each of which may vary with chordwise location x. Note that the limiting cases of R(x) = 1 and C = 0 correspond to the uniformly-porous and non-porous panels, respectively. Expected values of the porosity parameter in low-speed applications in air are $\delta = O(10^{-2})$, as measured experimentally by Geyer et al. (2010) and analyzed by Hajian and Jaworski (2017b). The pressure distributions for δ values of this magnitude do not show appreciable differences when compared to the nonporous case. Therefore, larger values of δ are considered here to illustrate more clearly the effects of increasing porosity, which could also be relevant to applications or future experiments in heavier fluids or faster flows.

Hajian and Jaworski (2019, 2017a) determined the non-circulatory forces on a vibrating panel in a single-sided flow with a prescribed chordwise porosity gradient. We recall from their work the following singular integral equation for pressure distribution over a panel with porosity distribution R(x):

$$p(x,t) = \frac{\delta}{\pi} \left(\int_0^1 \frac{R(\xi)p(\xi,t)}{x-\xi} \, \mathrm{d}\xi + 2 \frac{\sqrt{\mu_m}}{\lambda} \frac{\partial}{\partial t} \int_0^1 R(\xi)p(\xi,t) \ln|x-\xi| \, \mathrm{d}\xi \right) + f(x,t), \tag{4}$$

where

$$f(x,t) = \frac{2}{\pi} \left(\int_0^1 \frac{g(\xi,t)}{x-\xi} \, \mathrm{d}\xi + \frac{\sqrt{\mu_m}}{\lambda} \frac{\partial}{\partial t} \int_0^1 \left(g(\xi,t) + \frac{\sqrt{\mu_m}}{\lambda} \frac{\partial z_a}{\partial t} \right) \ln|x-\xi| \, \mathrm{d}\xi \right), \tag{5}$$

$$g(x,t) = \frac{\partial z_a}{\partial x} + \frac{\sqrt{\mu_m}}{\lambda} \frac{\partial z_a}{\partial t}.$$
 (6)

Here, $\mu_m = \rho l/\rho_s h$ is the mass ratio, and the dashed integral symbols denote a Cauchy principal value integral. The steady and unsteady solutions to Eq. (4) from Hajian and Jaworski (2017b, 2019) are presented in Sections 3 and 4, respectively.

3. Generalized aeroelastic divergence problem

Prior theoretical investigations (Ishii, 1965; Gislason, 1971) identify divergence as the primary aeroelastic instability of flexible, non-porous panels that are fixed at both ends. The critical flow velocity at which divergence occurs can be found by analyzing the panel static stability under steady aerodynamic forces (Kornecki et al., 1976). It should be noted that a dynamic (flutter) analysis is required to prove that divergence is indeed the primary form of instability, and such an analysis will be presented in the next section.

To study the divergence for porous panels, the time-dependent terms may be omitted from Eq. (4), which leads to the following integral equation for the pressure distribution p_{cr} on the panel occurring at the critical flow speed:

$$p_{\rm cr}(x) = \frac{\delta}{\pi} \int_0^1 \frac{R(\xi) p_{\rm cr}(\xi)}{x - \xi} \, \mathrm{d}\xi + \frac{2}{\pi} \int_0^1 \frac{\mathrm{d}z_a / \mathrm{d}\xi}{x - \xi} \, \mathrm{d}\xi. \tag{7}$$

This expression can be recast into the following canonical form that admits a general solution:

$$p_{\rm cr}(x) + \frac{\delta R(x)}{\pi} \int_0^1 \frac{p_{\rm cr}(\xi)}{\xi - x} \, \mathrm{d}\xi + \frac{1}{\pi i} \int_0^1 K(x, \xi) p_{\rm cr}(\xi) \, \mathrm{d}\xi = -\frac{2}{\pi} y(x), \tag{8}$$

where

$$K(x,\xi) = \frac{\mathrm{i}\delta\left[R(\xi) - R(x)\right]}{\xi - x},\tag{9}$$

and

$$y(x) = \int_0^1 \frac{\mathrm{d}z_a/\mathrm{d}\xi}{\xi - x} \,\mathrm{d}\xi = z_a'(1)\ln(1 - x) - z_a'(0)\ln x - \int_0^1 \frac{\mathrm{d}^2 z_a}{\mathrm{d}\xi^2} \ln|\xi - x| \,\mathrm{d}\xi. \tag{10}$$

Singular integral equation (8) can be recast as a Fredholm integral equation of the second kind (Muskhelishvili, 1953), which admits a solution in the form of a Liouville–Neumann series. As discussed in Hajian and Jaworski (2019), the Liouville–Neumann series converges rapidly for small porosity values of aerospace interest, i.e. $\delta = O(10^{-2})$. Therefore, the solution of Eq. (8) is approximated well by the first term of the series (Hajian and Jaworski, 2019):

$$p_{\rm cr}(x) \approx -\frac{2 y(x)}{\pi [1 + \delta^2 R^2(x)]} + \frac{2 \delta R(x)}{\pi^2 [1 + \delta^2 R^2(x)]} \left(\frac{x}{1 - x}\right)^{\frac{1}{\pi} \tan^{-1} \delta R(x)} \int_0^1 \frac{y(\xi)}{\xi - x} \left(\frac{1 - \xi}{\xi}\right)^{\frac{1}{\pi} \tan^{-1} \delta R(x)} d\xi. \tag{11}$$

To obtain the critical value of the nondimensional flow velocity λ , Eq. (11) is substituted into the equation of panel motion (2). Consideration of only the static stability under steady aerodynamic forces reduces the panel motion equation to

$$\frac{d^4 z_a}{dx^4} - \frac{\lambda^2}{\pi} \left[-\frac{y(x)}{1 + \delta^2 R^2(x)} + \frac{\delta R(x)}{1 + \delta^2 R^2(x)} \left(\frac{x}{1 - x} \right)^{\frac{1}{\pi} \tan^{-1} \delta R(x)} \int_0^1 \frac{y(\xi)}{\pi(\xi - x)} \left(\frac{1 - \xi}{\xi} \right)^{\frac{1}{\pi} \tan^{-1} \delta R(x)} d\xi \right] = 0.$$
 (12)

The special case of Eq. (12) for non-porous panels ($\delta = 0$) recovers the result derived previously by Kornecki et al. (cf. Eq. (14) in Kornecki et al., 1976).

3.1. Divergence instability for uniformly-porous panels

This section studies the divergence instability of uniformly-porous panels, for which R(x) = 1 in Eq. (7) for the pressure distribution at the onset of divergence. Following the procedure described in Muskhelishvili (1953), a set of auxiliary functions to solve for $p_{cr}(x)$ may be defined as follows:

$$G(x) = \frac{1 - \delta i}{1 + \delta i},\tag{13}$$

$$\Gamma(x) = \frac{1}{2\pi i} \int_{-1}^{1} \frac{\log G(t)}{t - x} dt = -k(\delta) \ln\left(\frac{1 - x}{x}\right),\tag{14}$$

where $k(\delta) = (\tan^{-1} \delta)/\pi$ for real δ that are assumed in this work, and the fundamental function Z(x) of the singular integral equation (7) is

$$Z(x) = \frac{\sqrt{1+\delta^2}}{2} \left(\frac{x}{1-x}\right)^{k(\delta)}.$$
 (15)

Substitution of Eqs. (13)–(15) into the general solution given by Eq. (47.13) in Muskhelishvili (1953) yields the following $p_{cr}(x)$ for uniformly-porous panels:

$$p_{cr}(x) = -\frac{2y(x)}{\pi(1+\delta^2)} + \frac{2\delta}{\pi^2(1+\delta^2)} \left(\frac{x}{1-x}\right)^{k(\delta)} \int_0^1 \frac{y(\xi)}{\xi - x} \left(\frac{1-\xi}{\xi}\right)^{k(\delta)} d\xi.$$
 (16)

Note that when considering R(x) = 1, the single-term series solution approximation (Eq. (11)) matches the exact solution Eq. (16) for uniformly-porous panels, since the higher-order terms in the Liouville-Neumann series reflect the effect of chordwise variation of the porosity function R(x) (Hajian and Jaworski, 2019).

To determine the critical flow velocity at which divergence occurs for uniformly-porous panels, Eq. (16) is now substituted into the equation of panel motion (2). Consideration of only the static stability under steady aerodynamic forces reduces the equation of panel motion to

$$\frac{\mathrm{d}^4 z_a}{\mathrm{d}x^4} - \frac{\lambda^2}{\pi} \left[-\frac{y(x)}{1+\delta^2} + \frac{\delta}{\pi(1+\delta^2)} \left(\frac{x}{1-x} \right)^{k(\delta)} \int_0^1 \frac{y(\xi)}{\xi - x} \left(\frac{1-\xi}{\xi} \right)^{k(\delta)} \mathrm{d}\xi \right] = 0. \tag{17}$$

Again, the special case of (17) for non-porous panels ($\delta = 0$) recovers the expression derived by Kornecki et al. (1976).

A uniformly-porous panel is now considered with a static deformation $z_a(x) = X(x)$ and its associated nondimensional pressure distribution p(x). Eq. (17) is solved using the Galerkin's method using a single structural mode to find the critical nondimensional dynamic pressure, λ^2 , at which divergence occurs for simply-supported and clamped ends. For the case of non-porous panels, this approach yields $\lambda_0^2 = 40.07$ for simply-supported ends, which agrees well with previous single-term analyses (Ellen, 1973; Kornecki et al., 1976) and the exact solution by Ishii (1965). Similarly, divergence occurs for clamped ends at $\lambda_0^2 = 180.9$, which is in close agreement with other works (Ellen, 1972; Kornecki et al., 1976). These critical dynamic pressure values for the non-porous panel are used to normalize the divergence trends in Fig. 2 for clamped and simply-supported panels as a function of the porosity parameter, δ . For both end conditions, an increase in δ leads to an increase in the critical dynamic pressure. Therefore, the divergence instability occurs at higher flow speeds, and the role of porosity is to suppress the onset of instability. Also, the normalized results in Fig. 2 demonstrate that the clamped end condition is comparatively more stable for increasing δ with respect to the simply-supported results, but the normalized critical dynamic pressure trends for both end conditions are approximately the same for small values of δ that are of practical interest in low-speed flows.

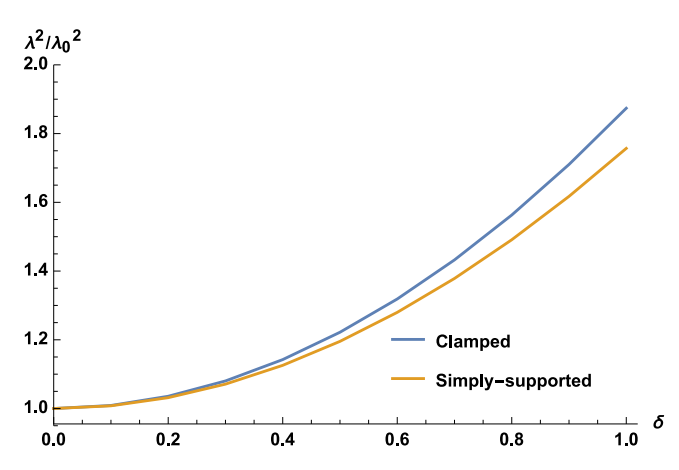


Fig. 2. Critical dynamic pressure for different values of porosity constants δ for panels with clamped ends, $X(x) = x^4 - 2x^3 + x^2$, and simply-supported ends, $X(x) = \sin(\pi x)$. The critical dimensionless dynamic pressures are normalized by the associated results for clamped ($\lambda_0^2 = 180.9$) and simply-supported ($\lambda_0^2 = 40.07$) end conditions.

4. Dynamic instability analysis for porous panels

The critical flow speed and frequency at which aeroelastic instability occurs are now examined for porous panels with harmonic motions, such that $z_a(x,t) = X(x)e^{i\omega t}$ and $p(x,t) = p(x)e^{i\omega t}$, where p(x) is a complex-valued function and ω is the complex dimensionless frequency that can be decomposed into a frequency and growth rate. The integral equation (4) can now be reduced and rearranged into the ordinary singular integral equation

$$p(x) + \frac{\delta R(x)}{\pi} \int_0^1 \frac{p(\xi)}{\xi - x} \, \mathrm{d}\xi + \frac{1}{\pi i} \int_0^1 K(x, \xi) p(\xi) \, \mathrm{d}\xi = f(x), \tag{18}$$

where

$$K(x,\xi) = 2\omega\delta \frac{\sqrt{\mu_m}}{\lambda} R(\xi) \ln|x - \xi| + i\delta \frac{R(\xi) - R(x)}{\xi - x},\tag{19}$$

$$f(x) = \frac{2}{\lambda^2} \left[\lambda^2 \tilde{I}_0(X, x) + i\omega\lambda\sqrt{\mu_m} \tilde{I}_1(X, x) - 2\mu_m \omega^2 \tilde{I}_2(X, x) \right]. \tag{20}$$

Note that Eq. (20) includes the effect of acoustic action on the lower panel surface, which, if neglected, would change the coefficient of the last term from 2 to 1. The functions \tilde{I}_0 , \tilde{I}_1 , and \tilde{I}_2 are defined by principal value integrals:

$$\tilde{I}_0(X,x) = \frac{1}{\pi} \int_0^1 \frac{X'(\xi)}{x - \xi} \, \mathrm{d}\xi,\tag{21}$$

$$\tilde{I}_{1}(X,x) = \frac{1}{\pi} \int_{0}^{1} \frac{X(\xi)}{x - \xi} + X'(\xi) \ln|x - \xi| \, \mathrm{d}\xi, \tag{22}$$

$$\tilde{I}_2(X,x) = \frac{1}{\pi} \int_0^1 X(\xi) \ln|x - \xi| \, \mathrm{d}\xi, \tag{23}$$

which are fundamental to the analysis of non-porous panels (Kornecki et al., 1976).

Hajian and Jaworski (2019) solve Eq. (18) with a Liouville-Neumann series,

$$p(x) = \lim_{n \to \infty} \sum_{j=0}^{n} \left(\frac{-1}{\pi i}\right)^{j} u_j(x), \tag{24}$$

where

$$u_0(x) = F(x),$$

$$u_1(x) = \int_0^1 N(x, \xi_1) F(\xi_1) \, d\xi_1,$$
(25)

$$u_n(x) = \int_0^1 \cdots \int_0^1 N(x, \xi_1) N(\xi_1, \xi_2) \cdots N(\xi_{n-1}, \xi_n) F(\xi_n) d\xi_n \cdots d\xi_1.$$

The associated fundamental function is

$$Z(x) = \sqrt{1 + \delta^2 R^2(x)} \exp\left[\frac{-1}{\pi} \int_0^1 \frac{\tan^{-1}[\delta R(\xi)]}{\xi - x} d\xi\right],$$
 (26)

which defines the functions

$$N(x,\xi) = \frac{1}{1+\delta^2 R^2(x)} k(x,\xi) - \frac{\delta R(x)}{\pi [1+\delta^2 R^2(x)]} Z(x) \int_0^1 \frac{K(t,\xi)}{Z(t)(t-x)} dt,$$
(27)

$$F(x) = \frac{1}{1 + \delta^2 R^2(x)} f(x) - \frac{\delta R(x)}{\pi [1 + \delta^2 R^2(x)]} Z(x) \int_0^1 \frac{f(t)}{Z(t)(t - x)} dt.$$
 (28)

With the pressure distribution established by Eq. (24), the dynamic aeroelastic stability can now be examined using Eq. (1) in the case of harmonic panel motions:

$$\frac{d^4X(x)}{dx^4} - \omega^2 X(x) - \frac{\lambda^2}{2} p(x) = 0.$$
 (29)

As noted earlier, the noncirculatory pressure distribution p(x) is closely approximated by the first term of the Liouville–Neumann series, $p(x) \approx F(x)$. Therefore Eq. (29) can be written as

$$\frac{d^{4}X(x)}{dx^{4}} - \omega^{2}X(x) - \lambda^{2}I_{0}(X, x, \delta) - i\omega\lambda\sqrt{\mu_{m}}I_{1}(X, x, \delta) + 2\mu_{m}\omega^{2}I_{2}(X, x, \delta) = 0,$$
(30)

with

$$I_{i}(X, x, \delta) = \frac{\tilde{I}_{i}(X, x)}{1 + \delta^{2} R^{2}(x)} - \frac{\delta R(x)}{\pi \left[1 + \delta^{2} R^{2}(x)\right]} Z(x) \int_{0}^{1} \frac{\tilde{I}_{i}(X, \xi)}{Z(\xi)(\xi - x)} d\xi, \qquad i = 0, 1, 2.$$
(31)

Eq. (30) has a form that is identical to Eq. (32) in Kornecki et al. (1976), except for the fact that here an extra term of $\mu_m \omega^2 I_2(X, x, \delta)$ appears due to the retained effect of the acoustic action on the panel, and the integrals I_0 , I_1 , and I_2 include extra terms involving the porosity. Equations (21)–(23) are recovered from Eq. (31) in the non-porous limit when $\delta = 0$. The solution of Eq. (30) may be expressed by the series

$$X(x) = \sum_{n} C_n X_n(x), \tag{32}$$

where C_n are constants and $X_n(x)$ are the free-vibration beam modes (Young and Felgar, 1949),

$$X_n(x) = \cosh(\beta_n x) - \cos(\beta_n x) - \alpha_n \left[\sinh(\beta_n x) - \sin(\beta_n x) \right]. \tag{33}$$

Coefficients α_n and β_n are set by the boundary conditions and are tabulated in Appendix A for the first two modes of a clamped-clamped panel.

The substitution of Eq. (32) into Eq. (30) and subsequent application of Galerkin's method yield an infinite set of homogeneous algebraic equations for the constants C_n . These equations have a non-trivial solution, provided that the determinant of their coefficient matrix vanishes (Kornecki et al., 1976):

$$Det\left[-\omega^{2}(\delta_{ij}-2\mu_{m}D_{ij})-i\omega\lambda\sqrt{\mu_{m}}B_{ij}+\beta_{i}^{4}\delta_{ij}-\lambda^{2}A_{ij}\right]=0,$$
(34)

for $i, j = 1, 2, 3, \dots$ Here δ_{ij} denotes the Kronecker delta, and A, B, and D are square matrices whose elements are defined by

$$A_{ij} = \int_0^1 X_i(x) I_0(X_j, x, \delta) \, \mathrm{d}x, \tag{35}$$

$$B_{ij} = \int_0^1 X_i(x) I_1(X_j, x, \delta) \, \mathrm{d}x, \tag{36}$$

$$D_{ij} = \int_0^1 X_i(x) I_2(X_j, x, \delta) \, \mathrm{d}x. \tag{37}$$

Kornecki et al. (1976) identified the terms in A_{ij} to be proportional to the steady aerodynamic forces, B_{ij} to the Coriolis forces, and D_{ij} to the virtual mass of the air surrounding the oscillating panel.

4.1. Dynamic instability analysis for uniformly-porous panels

The characteristic equation (34) for ω is now evaluated numerically for given dimensionless flow velocity λ and corresponding frequency ω of baffled, vibrating panels with clamped ends. To solve Eq. (34), the value of the mass ratio μ_m is fixed, two terms in Eq. (32) are retained.

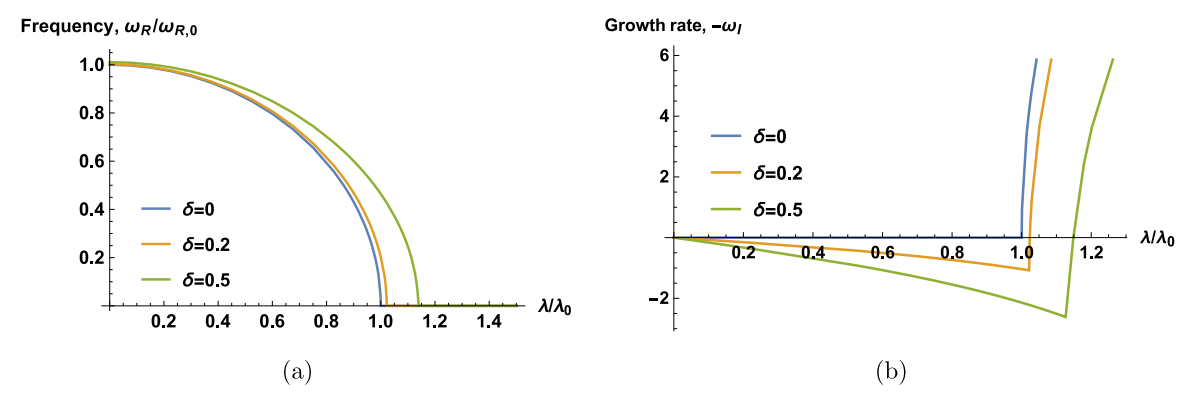


Fig. 3. Frequency and growth rate versus the dimensionless flow speed λ for a uniformly-porous panel with different values of the porosity parameter δ : (a) nondimensional frequency, $\omega_R/\omega_{R,0}$; (b) growth rate, $-\omega_I$. The plot axes are normalized where indicated by the critical value $\lambda_0 = 13.31$ of the non-porous panel and frequency $\omega_{R,0} = 20.31$ at $\lambda = 0$ for $\delta = 0$.

The metric of interest is the lowest value of λ for which the aeroelastic system becomes unstable. Physically, λ must be real and positive, but the frequency ω is a complex number, $\omega = \omega_R + \mathrm{i}\omega_I$, where ω_R and $-\omega_I$ indicate the frequency and growth rate, respectively. The aeroelastic stability boundary is defined by the critical flow velocity λ , beyond which one or more roots of Eq. (34) become unstable, i.e. $\omega_I > 0$. In the solution of Eq. (34), different values of porosity constants δ will be considered to examine the effects of porosity on the critical flow velocity.

Eq. (34) has been solved for $\mu_m=0.25$, whose value is of no consequence in this case, as will be discussed below. Fig. 3 shows the frequency and growth rate of the root that becomes unstable first as a function of λ for non-porous panels with clamped ends, which are compared against the cases of uniformly-porous panels with porosity constants $\delta=0.2$ and $\delta=0.5$. These results show that the first root loses stability by divergence for non-porous as well as porous panels. However, the critical value of λ and therefore the flow speed at which the panel becomes aeroelastically unstable is larger for porous panels, i.e., porous panels maintain aeroelastic stability at higher flow speeds before divergence occurs. This observation indicates that porosity acts to damp perturbed or vibrating panels. Note that the mass ratio μ_m does not affect the value of the critical dynamic pressure because the primary instability is divergence. The independence of the divergence criterion with respect to the mass ratio is obviated by Eq. (17), since μ_m does not appear in the static aeroelastic equations.

4.2. Effect of chordwise porosity distribution

In this subsection, the effects of the chordwise porosity variation R(x) on the divergence speed is investigated for five different porosity distributions that are plotted in Fig. 4. The constant, linear, and quadratic distributions are defined to have a maximum value of unity. Fig. 5 illustrates the frequency and growth rate versus the dimensionless flow velocity

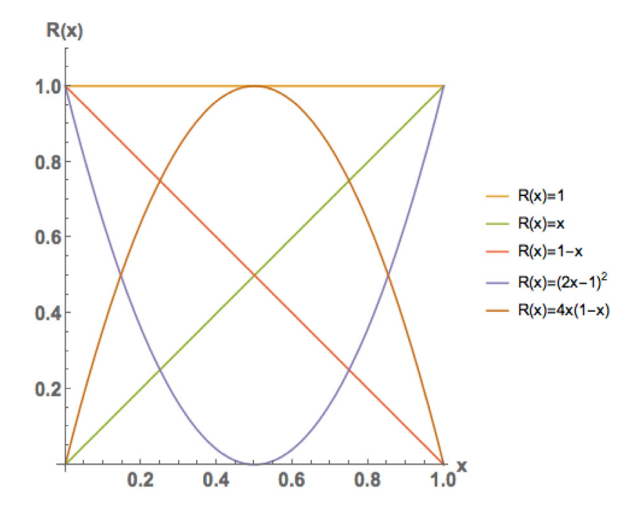


Fig. 4. Chordwise porosity distributions R(x).

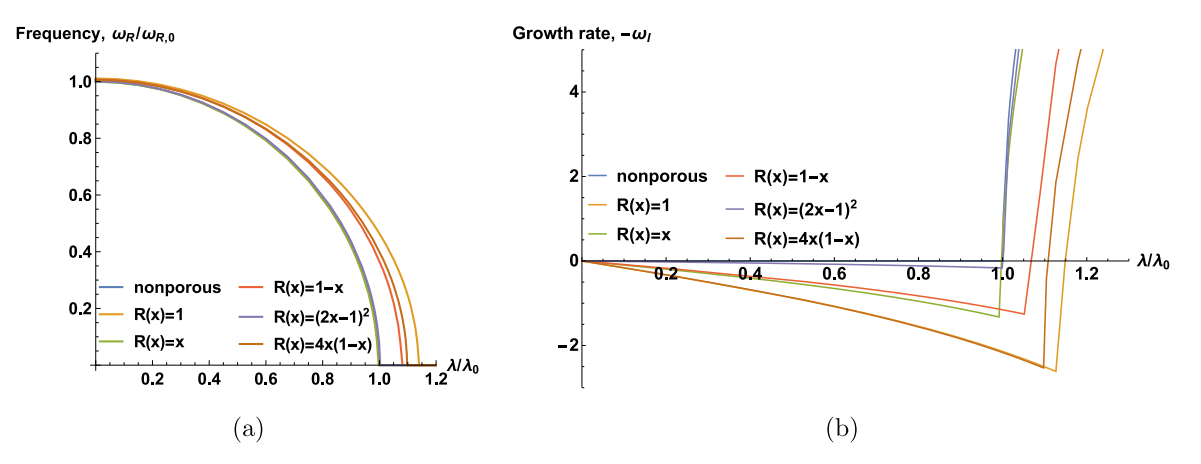


Fig. 5. Frequency and growth rate versus the dimensionless flow speed λ for different porosity distributions R(x) with $\delta = 0.5$: (a) nondimensional frequency, $\omega_R/\omega_{R,0}$; (b) growth rate, $-\omega_I$. The plot axes are normalized where indicated by the critical value $\lambda_0 = 13.31$ of the non-porous panel and frequency $\omega_{R,0} = 20.31$ at $\lambda = 0$ for $\delta = 0$.

for panels with clamped ends with these porosity distributions for fixed porosity parameter $\delta=0.5$. The axes of these plots are normalized by the critical value $\lambda_0=13.31$ of the non-porous panel and its frequency $\omega_{R,0}=20.31$ at $\lambda=0$. These values are consistent with the result presented in Eq. (28) in Kornecki et al. (1976). Note that the critical value of $\lambda=13.452$ was obtained in Section 3 for non-porous panels, which is the same as obtained result in Eq. (27) in Kornecki et al. (1976). The difference between these two values comes from the fact that in Section 3 only one mode is used to obtain the result, whereas two beam modes are used presently. Based on the results presented in Fig. 5, the details of the porosity distribution function R(x) at the trailing edge are crucial to determine the stability of a porous panel. Accordingly, for non-uniform porosity functions, decreasing the porosity distribution at the trailing edge, with negative derivative, imposes greater stability on the system. However, the most stable configuration is the uniformly-porous panel, which sets the upper bound for the divergence speed of porous panels with fixed δ . This conclusion holds for panels that are compared with respect to the porosity parameter δ . However, it is possible to construct other metrics to compare porosity (such as an integrated value, $\int_0^1 \delta R(x) dx$) where comparisons under such metrics may indeed lead to different conclusions.

4.3. Aeroelastic stability analysis using the Routh-Hurwitz stability criterion

The identification of divergence as the general primary aeroelastic instability mode is now examined rigorously for uniformly-porous panels, although the outlined procedure may also be applied in the general case of panels with chordwise porosity gradients. Introducing the parameter $s = i\omega$, Eq. (34) can be written in the form:

$$a_4 s^4 + \lambda \sqrt{\mu_m} a_3 s^3 + a_2 s^2 + \lambda \sqrt{\mu_m} a_1 s + a_0 = 0, \tag{38}$$

where

$$a_{4} = 1 - 2\mu_{m} \left(D_{11} + D_{22} \right) + 4\mu_{m}^{2} \left(D_{11}D_{22} - D_{12}D_{21} \right),$$

$$a_{3} = -B_{11} - B_{22} + 2\mu_{m} \left(B_{22}D_{11} - B_{21}D_{12} - B_{12}D_{21} + B_{11}D_{22} \right),$$

$$a_{2} = \beta_{1}^{4} + \beta_{2}^{4} - \lambda^{2} \left(A_{11} + A_{22} \right) - 2\mu_{m} \left(D_{22}\beta_{1}^{4} + D_{11}\beta_{2}^{4} \right)$$

$$-\lambda^{2} \mu_{m} \left(B_{12}B_{21} - B_{11}B_{22} - 2A_{22}D_{11} + 2A_{21}D_{12} + 2A_{12}D_{21} - 2A_{11}D_{22} \right),$$

$$a_{1} = -B_{22}\beta_{1}^{4} - B_{11}\beta_{2}^{4} + \lambda^{2} \left(A_{22}B_{11} - A_{21}B_{12} - A_{12}B_{21} + A_{11}B_{22} \right),$$

$$a_{0} = \beta_{1}^{4}\beta_{2}^{4} - \lambda^{2} \left(A_{22}\beta_{1}^{4} + A_{11}\beta_{2}^{4} \right) + \lambda^{4} \left(A_{11}A_{22} - A_{12}A_{21} \right).$$

$$(39)$$

The values of a_i coefficients for the representative porosity cases considered here ($\delta = 0, 0.2, 0.5$) are presented in Tables 1–3 in Appendix B. The aeroelastic stability is determined by sweeping through positive values of λ and solving for the roots s of the characteristic equation (38) until the neutrally-stable condition is found. At the neutrally-stable condition, the instability is flutter if the associated complex root s has a non-zero imaginary part, and divergence occurs if this imaginary component is identically zero (Dugundji et al., 1963).

The instability of the aeroelastic system can be assessed from the coefficients of the quartic polynomial (38) by appeal to the *Routh–Hurwitz stability criterion* (Dorf and Bishop, 2011), which is a necessary and sufficient condition for the

stability of a characteristic equation without solving for the roots directly. According to this criterion, the aeroelastic system is stable if all of the following conditions are satisfied simultaneously:

$$\begin{cases}
 a_i > 0, & \text{for } i = 0, 1, 2, 3, \\
 a_2 a_3 - a_1 a_4 > 0, \\
 a_1 a_2 a_3 - a_4 a_1^2 + a_0 a_3^2 > 0.
\end{cases}$$
(40)

Here we may assume $a_4 > 0$ without loss of generality with respect to the onset of aeroelastic instability.

When applying this stability criterion to uniformly-porous panels with $\delta=0$, 0.2, 0.5 (cf. Appendix B), it is observed that all of the conditions are satisfied in the absence of a flow, $\lambda=0$. As the flow speed increases, the sign change of a_0 is the first condition to be violated in all cases considered. Thus, at the neutrally-stable condition $a_0=0$ and Eq. (38) produces s=0, the root associated with divergence. Therefore, the divergence instability is analytically established for uniformly-porous airfoils using only the signs of six terms. This method can also be applied to panels with variable porosity distributions, where this variation is embedded in the coefficients a_i .

5. Conclusion

Static and dynamic aeroelastic stability analyses are carried out for baffled porous panels with chordwise-varying porosity distributions. These analyses confirm that divergence is the primary aeroelastic stability of both porous and non-porous panels. This result is shown to be robust to the details of the magnitude and chordwise distribution of the Darcy-type porosity condition. The generality of the divergence instability for porous panels is demonstrated analytically using the Routh–Hurwitz stability criterion.

Increasing the panel porosity with respect to the dimensionless porosity parameter δ has a stabilizing effect when compared to divergence speed of the non-porous panel and occurs for both clamped and simply-supported ends. The divergence speed is shown to depend on the definition of the chordwise porosity distribution, where a uniformly-porous panel establishes the upper stability limit. Therefore, the effect of porosity on panels in low-speed flows is to suppress the aeroelastic divergence instability, which may be advantageous in the practical design of compliant panels and porous liners.

Acknowledgment

This work was financially supported by the National Science Foundation under grant award 1805692, monitored by Dr. R. Joslin.

Declaration of competing interest

The authors declare that they have no known competing financial interests or personal relationships that could have appeared to influence the work reported in this paper.

CRediT authorship contribution statement

Rozhin Hajian: Conceptualization, Methodology, Writing — original draft. **Justin W. Jaworski:** Writing — review & editing, Supervision, Funding acquisition.

Appendix A. Boundary condition constants for beam modes

The following constants from Young and Felgar (1949) define the first two clamped-clamped beam modes of Eq. (33).

 $\alpha_1 = 0.9825022158, \quad \beta_1 = 4.7300408$ $\alpha_2 = 1.000777311, \quad \beta_2 = 7.8532046$

Appendix B. Aeroelastic stability coefficients for porous panels

The values of a_i coefficients in Eq. (39) for different values of the porosity parameter δ are presented in Tables 1–3.

Table 1 coefficients for non-norms namels $\delta = 0$

u_i coefficients for non-porous paners, $v = 0$.	
a_0	$1.90391\times 10^6 - 13890.5\lambda^2 + 17.7704\lambda^4$
a_1	0
a_2	$4304.1 - 9.11693\lambda^2 + 3439.24\mu_m - 4.3433\mu_m\lambda^2$
a_3	0
a_4	$1 + 1.2489\mu_m + 0.338164\mu_m^2$

Table 2 a_i coefficients for uniformly-porous panels with $\delta = 0.2$.

	• • • • • • • • • • • • • • • • • • • •
a_0	$1.90391\times 10^6 - 13397.2\lambda^2 + 16.9317\lambda^4$
a_1	$1192.01 - 0.747522\lambda^2$
a_2	$4304.1 - 8.77767\lambda^2 + 3359.03\mu_m - 4.09922\lambda^2\mu_m$
a_3	$0.636395 + 0.191058\mu_m$
a_4	$1 + 1.21538\mu_m + 0.32457\mu_m^2$

Table 3 a_i coefficients for uniformly-porous panels with $\delta = 0.5$.

a_0	$1.90391 \times 10^6 - 11302.1\lambda^2 + 13.5212\lambda^4$
a_1	$2534.13 - 1.35312\lambda^2$
a_2	$4304.1 - 7.34557\lambda^2 + 3008.5\mu_m - 3.12321\lambda^2\mu_m$
a_3	$1.34087 + 0.36924 \mu_m$
a_4	$1 + 1.07052\mu_m + 0.267862\mu_m^2$

References

Biot, M.A., 1956. The divergence of supersonic wings including chordwise bending. J. Aeronaut. Sci. 23 (3), 237-252.

Bisplinghoff, R.L., Ashley, H., Halfman, R.L., 1996. Aeroelasticity. Dover Publications, New York.

Corkery, S.I., Babinsky, H., Graham, W.R., 2019. Quantification of added-mass effects using particle image velocimetry data for a translating and rotating flat plate. J. Fluid Mech. 870, 492-518.

Datta, S.K., Gottenberg, W.G., 1975. Instability of an elastic strip hanging in an airstream. J. Appl. Mech. 42, 195-198.

Dorf, R.C., Bishop, R.H., 2011. Modern Control Systems. Pearson.

Dowell, E.H., 1974. Aeroelasticity of Plates and Shells. Noordhoff.

Dugundji, J., Dowell, E., Perkin, B., 1963. Subsonic flutter of panels on continuous elastic foundations. AIAA J. 1 (5), 1146-1154.

Eldredge, J.D., 2010. A reconciliation of viscous and inviscid approaches to computing locomotion of deforming bodies. Exp. Mech. 50, 1349-1353.

Ellen, C.H., 1972. Stability of clamped rectangular plates in uniform subsonic flow. AIAA J. 10 (12), 1716-1717.

Ellen, C.H., 1973. The stability of simply supported rectangular surfaces in uniform subsonic flow. J. Appl. Mech. 40 (1), 68-72.

Fahy, F., Gardonio, P., 2007. Sound and Structural Vibration: Radiation, Transmission and Response, second ed. Elsevier.

Fox, C., 1950. An Introduction to the Calculus of Variations. Courier Corporation.

Geyer, T., Sarradi, E., Fritzsche, C., 2010. Measurement of the noise generation at the trailing edge of porous airfoils. Exp. Fluids 48 (2), 291-308.

Gislason, T., 1971. Experimental investigation of panel divergence at subsonic speeds. AIAA J. 9 (11), 2252-2258.

Graham, W.R., Pitt Ford, C.W., Babinsky, H., 2017. An impulse-based approach to estimating forces in unsteady flow. J. Fluid Mech. 815, 60-76. Hajian, R., Jaworski, J.W., 2015. The steady aerodynamics of quiet airfoils with porosity gradients. In: 45th AIAA Fluid Dynamics Conference, Dallas,

TX. Paper AIAA-2015-2304.

Hajian, R., Jaworski, J.W., 2017a. Non-circulatory fluid forces on panels and airfoils with porosity gradients. In: 8th AIAA Theoretical Fluid Mechanics Conference, Denver, CO, Paper AIAA-2017-4339.

Hajian, R., Jaworski, J.W., 2017b. The steady aerodynamics of aerofoils with porosity gradients. Proc. R. Soc. Lond. Ser. A Math. Phys. Eng. Sci. 473

Hajian, R., Jaworski, J.W., 2019. Noncirculatory fluid forces on panels with porosity gradients. AIAA J. 57 (2), 870-875.

Hedgepeth, J.M., 1957. Flutter of rectangular simply supported panels at high supersonic speeds. J. Aeronaut. Sci. 24 (8), 563-573.

Ishii, T., 1965. Aeroelastic instabilities of simply supported panels in subsonic flow. In: Aircraft Design and Technology Meeting, p. 772.

Jacobsen, F., Juhl, P.M., 2013. Fundamentals of General Linear Acoustics, first ed. Wiley.

Jolly, M.R., Sun, J.Q., 1994. Passive tuned vibration absorbers for sound radiation attenuation from panels. In: Smart Structures and Materials 1994: Passive Damping, Vol. 2193. International Society for Optics and Photonics, pp. 194-202.

Kornecki, A., Dowell, E.H., O'Brien, J., 1976. On the aeroelastic instability of two-dimensional panels in uniform incompressible flow. J. Sound Vib. 47 (2), 163-178.

Leonard, A., Roshko, A., 2001. Aspects of flow-induced vibration. J. Fluids Struct. 15, 415-425.

Muskhelishvili, N.I., 1953. Singular Integral Equations. Noordhoff, Groningen.

Theodorsen, T., 1949. General Theory of Aerodynamic Instability and the Mechanism of Flutter. NACA Report 496.

Weaver, D.S., Unny, T.E., 1970. The hydroelastic stability of a flat plate. J. Appl. Mech. 37 (3), 823-827.

Wright, R.I., Kidner, M.R.F., 2004. Vibration absorbers: A review of applications in interior noise control of propeller aircraft. J. Vib. Control 10 (8), 1221-1237.

Young, D., Felgar, R.P., 1949. Tables of Characteristic Functions Representing Normal Modes of Vibration of a Beam. Tech. Rep. 4913, University of Texas at Austin.